AKUSTICKÉ LISTY

České akustické společnosti
www.czakustika.cz

ročník 23, číslo 1–4 prosinec 2017

Obsah

ČESKÁ AKUSTICKÁ SPOLEČNOST

13. srpna 2017 zemřel Ing. Jan Kozák, CSc.

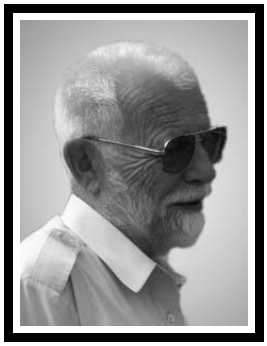

Honza, jak byl vždy jmenován mezi přáteli, byl po ukončení vysoké školy zaměstnán ve Státním výzkumném ústavu pro stavbu strojů v Běchovicích, kde se věnoval akustice a chvění a v této oblasti dosahoval vynikajících výsledků. Po roce 1990 se tímto oborem zabýval na Ministerstvu životního prostředí. Jeho zaměření na hluk strojních zařízení a později na dopravní hluk bylo velkým přínosem pro danou problematiku, ať už z hlediska aplikovaného výzkumu a vývoje, nebo z hlediska vzdělávání „akustiků-hlukařů“ v praxi. Dlouhá léta byl lektorem a organizátorem kurzů, kde se svými přednáškami zapsal do povědomí snad všech absolventů. Byl autorem mnoha odborných článků a studijních materiálů odborných kurzů, přeložil do češtiny celou řadu norem. Mimo své pracovní povinnosti byl též velmi aktivní ve Vědeckotechnické společnosti v sekci hluk prostředí a později v České akustické společnosti, kde až do svého odchodu působil v radě společnosti a podílel se na tvorbě Akustických listů. Byl jedním ze zakladatelů akustických seminářů, kde byl vždy velmi aktivní ať již jako pořadatel, nebo posluchač či přednášející. Zvuk zvonečku, který ohlašuje začátek přednášek, nám ho bude navždy připomínat. Pro svoji povahu byl Honza mezi přáteli vždy velmi oblíben, uměl se vypořádat s problémy a nikdy nikoho nezarmucoval. Bohužel již není mezi námi a bude celé akustické obci chybět. Honzíku, budeme na Tebe vždy v dobrém vzpomínat.

Bývalí spolupracovníci.

Fenomenologický model generování zvuku ve vroubkovaných trubicích a jeho modální řešení

Phenomenological Model of Sound Generation in a Corrugated Pipe and its Modal Solution

Viktor Hruška a Michal Bednařík

České vysoké učení technické v Praze, Fakulta elektrotechnická, Technická 2, 166 27 Praha 6

Phenomenological model of sound generation in a corrugated pipe is established along with its motivation from the aeroacoustic wave equations. Numerical simulations show very good correspondence with desired nonlinear system features such as mode-locking and hysteresis.

1. Úvod

Ohebná vroubkovaná hadice („husí krk“, angl. currugated pipe nebo rovněž „gooseneck“) dnes představuje neodmyslitelnou součást inženýrských instalací od centimetrových škál v domácnostech po podvodní vedení v řádu stovek metrů (flexible risers). Její hlavní předností je celková ohebnost při zachování lokální pevnosti. Vedlejší efekt představují turbulentní struktury v proudění v blízkosti vroubků, které mohou generovat zvuk. Kromě nežádoucí emise hluku může zvuk díky vazbě na rezonátor dosáhnout akustických tlaků nebezpečných pro samotnou strukturu trubice [1].

Místo náročné formulace odvozené z Navierových-Stokesových rovnic představujeme pokročilejší verzi fenomenologického modelu, který formuloval Debut a kol. [2]. Ten se opírá o popis nelineárního chování nestacionárního toku v turbulentní mezní vrstvě pomocí van der Polových rovnic (dále např. [3, 4]), na rozdíl od přímé simulace (např. [5]) nebo zjednodušených akustických modelů (např. [6, 7]). Shrnutí starší literatury viz [1].

V dalším textu je nejprve shrnuta teorie, včetně motivace pro fenomenologický přístup (část Modelové rovnice). Následující partie obsahují výsledky řešení rovnic (část Numerické simulace), posouzení jejich platnosti a korespondenci s experimentálními výsledky (Diskuze a Závěr).

2. Modelové rovnice

Teoretické východisko představuje zobecnění Lighthillovy akustické analogie pro proudění v blízkosti pevných struktur: Curleova analogie. Mějme v proudění o rychlostech $\boldsymbol{v}(\boldsymbol{x}, t)$ nepohyblivé tuhé těleso ohraničené plochou S definovanou pomocí rovnice typu $g(\boldsymbol{x}) = 0$. Zavedeme Heavisideovu funkci $\mathrm{H}(g)$ tak, že $\mathrm{H} = 1$ vně plochy S a $\mathrm{H} = 0$ uvnitř. Dále předpokládejme malá Machova čísla (nestlačitelné proudění) a vysoká Reynoldsova čísla (malý vliv viskozity). Pak pro malé poruchy hustoty v tekutině platí vlnová rovnice (zápis v Einsteinově notaci) [8]:

$$\left(\frac{1}{c_0^2}\frac{\partial^2}{\partial t^2} - \nabla^2\right)\left[\mathrm{H}\, c_0^2\,(\rho - \rho_0)\right] = \frac{\partial^2\,(\mathrm{H} R_{ij})}{\partial x_i \partial x_j} - \frac{\partial}{\partial x_i}\left[\left(R_{ij} + p'_{ij}\right)\frac{\partial \mathrm{H}}{\partial x_j}\right], \quad (1)$$

kde $p'_{ij} = (p - p_0)\,\delta_{ij} - \sigma_{ij}$ je tenzor kompresivního napětí (compressive stress tensor) a $p - p_0$ rozdíl rovnovážného a okamžitého tlaku, σ_{ij} je tenzor viskózních napětí a δ_{ij} je Kroneckerův symbol. Člen $R_{ij} = \rho_0 v_i v_j$ je úměrný Reynoldsovu tenzoru napětí, tedy míře přenosu hybnosti turbulentními fluktuacemi. Značení ρ, ρ_0, c_0 znamená jako obvykle okamžitou a klidovou hustotu a adiabatickou rychlost zvuku.

První člen na pravé straně v rovnici (1) odpovídá kvadrupólovým zdrojům, které představují turbulence ve volném poli, druhý člen potom dipólovému zdroji, který je následkem reakce tuhého tělesa na nestacionární hydrodynamické síly v jeho okolí. Další člen by přibyl, pokud bychom uvažovali vlastní objemovou pulzaci tělesa.

Pomocí Greenovy funkce lze získat integrální obdobu rovnice (1) a následně by bylo možné určit akustický tlak například z numerické simulace nestlačitelného proudění ve vroubkované hadici. Z energetického hlediska nepředstavuje tento přístup problém; lze ukázat, že ztráta kinetické energie toku kvůli akustickému vyzařování je pro potřeby modelování proudění zanedbatelně malá. Obtíže v přímé simulaci vznikají kvůli zpětnovazebním efektům. Potřeba uvažovat okrajové podmínky a výskyt odraženého zvuku významně komplikují integrální formulaci. Proudění kolem vroubku se navíc typicky kvalitativně pohybuje nad kritickým Reynoldsovým číslem, a je tedy velmi citlivé na poruchy ve svém okolí. V dosavadní literatuře už bylo ukázáno, že okamžitý charakter proudění uvnitř vroubku je do značné míry řízen okamžitým akustickým tlakem [3]. Zbývalo by tedy pouze náročné modelování pomocí Navierových-Stokesových rovnic pro stlačitelnou tekutinu.

Přijato 31. října 2017, akceptováno 30. listopadu 2017.

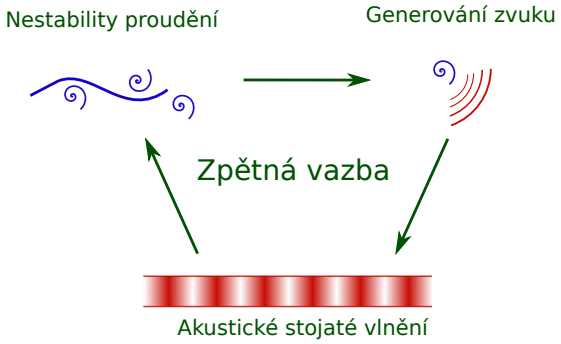

Obrázek 1: Zjednodušené schéma zpětnovazební smyčky mezi prouděním a akustickým polem v trubici

Z předchozích odstavců vyplývá, že vhodný fenomenologický model (obsahující potřebné kvalitativní chování zdroje) může být pro představu o akustickém chování systému prospěšnější než náročný numerický model platný jen pro konkrétní nastavení.

Představu o chování zdroje získáme pomocí Howeova vzorce pro akustický výkon generovaný tokem v blízkosti pevných těles [9]. Plné odvození zde nebude reprodukováno, ale pro zdůraznění souvislostí s Curleovou analogií si stačí uvědomit, že

$$\frac{\partial^2 R_{ij}}{\partial x_i \partial x_j} = \rho_0 \frac{\partial^2}{\partial x_i \partial x_j}\left(v_i v_j\right) = \rho_0 \nabla\cdot(\boldsymbol{\omega}\times\boldsymbol{v}) + \frac{\rho_0}{2}\nabla^2\left(v^2\right) \,, \quad (2)$$

kde $\boldsymbol{\omega} = \nabla \times \boldsymbol{v}$ je vířivost (vír rychlosti). Druhý člen na pravé straně vyzařuje oproti prvnímu zanedbatelně málo [10]. Střední akustický výkon $\langle \mathcal{P}_{\mathrm{ac}} \rangle$ generovaný nebo disipovaný v oblasti Ω je:

$$\langle \mathcal{P}_{\mathrm{ac}} \rangle = \left\langle \int_\Omega \rho_0 \left(\boldsymbol{\omega}\times\mathbf{v}\right)\cdot\nabla\phi' \,\mathrm{d}V \right\rangle \,, \quad (3)$$

kde ϕ' je odchylka rychlostního potenciálu od střední hodnoty (pro subsonická proudění je tedy $\nabla\phi'$ akustická rychlost).

Odtud plyne několik důležitých vlastností zdroje. Zvuk zpětnovazebně působí na svůj vlastní zdroj (viz obr. 1). Akustická energie může být generována i disipována, a je tedy rozumné předpokládat existenci saturovaného stavu systému, ve kterém budou obě tendence vyrovnány. Zvuk je generován převážně v oblastech s vysokými hodnotami akustické rychlosti, a naopak oblast uzlu akustické rychlosti by teoreticky měla být, co do vyzařování, pasivní. Člen $\rho_0\left(\boldsymbol{\omega}\times\mathbf{v}\right)$ je objemová hustota Coriolisovy síly. Odtud vyplývá důležitost unášení rotačních struktur v tekutině.

Této charakteristice je přizpůsoben fenomenologický model. Budeme uvažovat trubici jako jednorozměrnou (viz níže). Každý vroubek (resp. proudění v jeho těsné blízkosti) bude představovat diskrétní zdroj modelovaný jako van der Polův oscilátor s pravou stranou, která zajišťuje

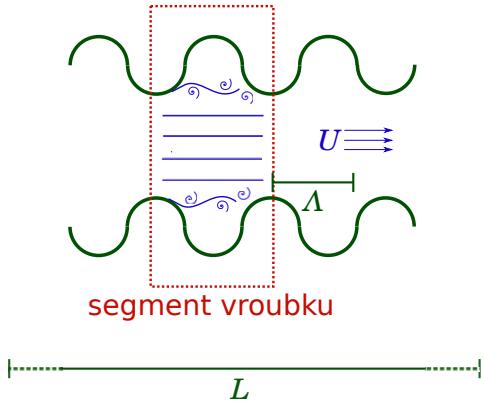

Obrázek 2: Zjednodušené schéma segmentu vroubkované trubice

vazbu na zvukové pole v trubici (schematicky viz obr. 1). Pro zdroj na n-tém vroubku platí [2]:

$$\frac{\mathrm{d}^2 P_n}{\mathrm{d}t^2} + A\,\omega_{\mathrm{S}}\left[\left(\frac{P_n}{BU^\alpha}\right)^2 - 1\right]\frac{\mathrm{d}P_n}{\mathrm{d}t} + \omega_{\mathrm{S}}^2 P_n = C\left.\frac{\partial p}{\partial x}\right|_{x=x_n} \,, \quad (4)$$

kde A, B, C a α jsou konstanty popsané níže, ω_{S} Strouhalova (úhlová) frekvence a $p(x,t)$ nyní značí akustický tlak. Proměnná $P_n(t)$ je ekvivalent zdrojového akustického tlaku, derivace akustického tlaku podle prostorové proměnné dává (s příslušnou konstantou) odhad lokální akustické rychlosti.

Strouhalovu frekvenci zavádíme ve tvaru:

$$\omega_{\mathrm{S}} = 2\pi\,\mathrm{St}\frac{U}{\Lambda} \,, \quad (5)$$

kde St je Strouhalovo číslo, U charakteristická rychlost proudění v trubici a Λ charakteristická délka, která bývá definována jako délka prohlubně mezi dvěma vroubky zvětšená o poloměr křivosti odtokové hrany vroubku [6].

Předpokládáme, že trubice má vzhledem ke znějící vlnové délce malý průměr, a tedy stačí vycházet z jednorozměrné vlnové rovnice. Jevy v mezní vrstvě jsou již popsány nelineárním tlumením ve van der Polově rovnici, takže vyjdeme z vlnové rovnice pro viskózní, tepelně vodivou tekutinu ve tvaru zahrnujícím jen objemové ztráty [11]:

$$\left(\tilde{V} + \frac{\gamma-1}{\mathrm{Pr}}\right)\frac{\mu}{\rho_0 c_0^2}\frac{\partial^3 u}{\partial x^2 \partial t} + \frac{\partial^2 u}{\partial x^2} - \frac{1}{c_0^2}\frac{\partial^2 u}{\partial t^2} = 0 \,, \quad (6)$$

kde $u(x,t)$ je akustická rychlost, γ adiabatický exponent, Pr Prandtlovo číslo, ρ_0 klidová hustota vzduchu, c_0 adiabatická rychlost zvuku, μ (dynamická) viskozita a $\tilde{V}$ viskózní číslo (korekce dynamické viskozity podle Stokesova předpokladu).

Předpokládáme šíření rovinných vln malých amplitud (tzn. vztah akustické rychlosti a tlaku je lineární), přidáme budicí člen, který odpovídá zdroji tlaku, a upravíme:

$$\frac{\partial^2 p}{\partial t^2} - c_0^2 \frac{\partial^2 p}{\partial x^2} = -\frac{\partial f}{\partial x} + \zeta \frac{\mu}{\rho_0} \frac{\partial^3 p}{\partial x^2 \partial t} \,, \tag{7}$$

kde $f(x,t)$ je objemová hustota budicí síly a $\zeta = \tilde{V} + \frac{\gamma-1}{\mathrm{Pr}}$. Zdrojový člen tvoří součet příspěvků od van der Polových oscilátorů, jehož prostorová část je modelována pomocí vzorkovací vlastnosti Diracovy funkce $\delta(x)$: $f(x,t) = \sum_n P_n(t)\,\delta(x - x_n)$. Odtud

$$\frac{\partial^2 p}{\partial t^2} - c_0^2 \frac{\partial^2 p}{\partial x^2} = - c_0^2 \sum_n P_n(t) \frac{\partial}{\partial x} \delta(x - x_n) + \zeta \frac{\mu}{\rho_0} \frac{\partial^3 p}{\partial x^2 \partial t} \,. \tag{8}$$

Efekty unášení zvukového pole střední rychlostí proudění vzduchu U, kterou považujeme za uniformní, postihneme pomocí transformace:

$$\frac{\partial}{\partial t} \to \frac{\mathrm{D}}{\mathrm{D}t} \equiv \frac{\partial}{\partial t} + U \frac{\partial}{\partial x} \,. \tag{9}$$

Pro vyšší derivace postupujeme analogicky. Dostáváme vlnovou rovnici ve tvaru:

$$\frac{\partial^2 p}{\partial t^2} - c_0^2 \frac{\partial^2 p}{\partial x^2} = -c_0^2 \sum_n P_n(t) \frac{\partial}{\partial x} \delta(x - x_n) - U \frac{\partial^2 p}{\partial x \partial t} - U^2 \frac{\partial^2 p}{\partial x^2} + \zeta \frac{\mu}{\rho_0} \frac{\partial^3 p}{\partial x^2 \partial t} + \zeta \frac{\mu}{\rho_0} U \frac{\partial^3 p}{\partial x^3} \,. \tag{10}$$

Soustava rovnic (4) a (10) představuje východisko pro další úpravy.

Předpokládáme, že vliv útlumu a vyzařování je natolik malý, abychom mohli akustický tlak v trubici délky L popsat jako součin M ortogonálních módů:

$$p(x,t) = \sum_{m=1}^{M} q_m(t) \sin \frac{m\pi x}{L} \,. \tag{11}$$

S využitím ortogonality (postup viz např. [12]) dostáváme soustavu obyčejných diferenciálních rovnic pro M modálních amplitud q_m a N van der polovských tlakových zdrojů P_n:

$$\ddot{q}_m + \zeta \frac{\mu}{\rho_0} \frac{m^2\pi^2}{L^2} \dot{q}_m + \left(\omega_m^2 - \frac{\pi^2 m^2 U^2}{L^2} \right) q_m = \frac{2m\pi c_0^2}{L^2} \sum_n P_n \cos \frac{m\pi x_n}{L} \,, \tag{12}$$

$$\ddot{P}_n + A\,\omega_S \left[\left(\frac{P_n}{B U^\alpha} \right)^2 - 1 \right] \dot{P}_n + \omega_S^2 P_n = - \frac{\pi C}{L} \sum_{m=1}^{M} m\, q_m \cos \frac{m\pi x}{L} \,, \tag{13}$$

zde tečka značí derivaci podle času. Rovnice převedeme do bezrozměrného tvaru zavedením bezrozměrného času τ, bezrozměrné frekvence ν, Machova čísla $\mathcal{M}$ a akustického Reynoldsova čísla $\mathrm{Re_a}$:

$$\omega_m = \frac{m\pi c_0}{L} \,, \qquad \tau = \omega_1 t = \frac{\pi c_0}{L} t \,,$$
$$\mathcal{M} = \frac{U}{c_0} \,, \qquad \nu = 2\mathcal{M}\,\mathrm{St} \frac{L}{\Lambda} \,,$$
$$\mathrm{Re_a} = \frac{\rho_0 c_0^2}{\omega \mu} = \frac{c_0 L}{m\pi\nu} \,, \qquad C = \omega_\mathrm{S} U \xi \,.$$

Vesměs se jedná o přímočaré definice bezrozměrných podobnostních čísel. Komentář k zavedení parametru ξ je uveden níže. Dostáváme:

$$\ddot{q} + \frac{m^2 \zeta}{\mathrm{Re_a}} \dot{q} + m^2 \left(1 - \mathcal{M}^2\right) q = \frac{2m}{\pi} \sum_{n=1}^{N} P_n \cos \frac{m\pi x_n}{L} \,, \tag{14}$$

$$\ddot{P} + A\,\nu \left[\left(\frac{P}{B c_0^\alpha \mathcal{M}^\alpha} \right)^2 - 1 \right] \dot{P} + \nu^2 P = - \nu \mathcal{M} \xi \sum_{m=1}^{M} m q_m \cos \frac{m\pi x_n}{L} \,, \tag{15}$$

zde tečka značí derivaci podle bezrozměrného času τ.

Odtud je zřejmé, že proudění má kromě zdrojových vlastností v tomto modelu vliv jen jako faktor $\left(1 - \mathcal{M}^2\right)$ mírně snižující vlastní frekvenci trubice. Tento efekt je ale zanedbatelně malý pro subsonické toky, a navíc pro vyšší hodnoty Machova čísla $\mathcal{M}$ už není možné použít výše uvedený teoretický základ, který stojí na předpokladu nestlačitelného proudění [8, 9].

Zbývá přiblížit fyzikální význam konstant A, B, C a α v rovnici (4). Konstanta A je spojována s poměrem tloušťky turbulentní mezní vrstvy ku poloměru trubice. Její hodnota by tak měla být výrazně menší než 1. Vazebná konstanta C by měla být závislá na poměru budicí frekvence k vlastní frekvenci vroubku (v přiblížení Helmholtzova rezonátoru). Odtud kvůli bezrozměrnému charakteru zavedení nové konstanty ξ tak, že $C = \omega_\mathrm{S} U \xi$.

Konstanty α a B nemají jednoznačný fyzikální význam a slouží především jako ponechaný stupeň volnosti k proložení experimentálních dat. Konstanta B řídí velikost limitního cyklu van der Polova oscilátoru, koeficient $\alpha \approx 2$, viz [3].

3. Numerické simulace

Za účelem demonstrace vlastností fenomenologického modelu byla pro numerické simulace zvolena trubice délky $L = 2$ m s 50 vroubky a 20 uvažovanými módy rezonance. Charakteristická hydrodynamická délka byla $\Lambda = 6$ mm, Strouhalovo číslo $\mathrm{St} = 0{,}4$, rychlost zvuku $c_0 = 340\,\mathrm{m{\cdot}s^{-1}}$,

vazebný koeficient $\xi = 0{,}01$, tlumení $\zeta/\mathrm{Re_a} = 0{,}001$ a konstanty $A = 0{,}005$, $B = 0{,}000\,1$ a $\alpha = 2$. Rovnice byly řešeny pomocí klasické Rungovy-Kuttovy metody 4. řádu. Počáteční akustický tlak a jeho časová derivace byly nulové, počáteční hodnoty P_n a jejich derivací byly voleny náhodné v $\mathcal{O}\left(10^{-4}\right)$. Fyzikálně tato volba odpovídá tiché tekutině v trubici s výkonově velmi slabými, nesynchronizovanými zdroji.

Se systémem byly provedeny dva typy simulací. Na obr. 3 je efekt lineárního nárůstu rychlosti (rychlostního sweepu). Okamžité frekvence a hladiny akustické rychlosti v ústí trubice (SVL) byly získány z výsledného signálu pomocí Hilbertovy transformace. Zjevná je zejména synchronizace znějící frekvence s vlastními frekvencemi trubice (mode lock-in). Uvedená hladina akustického tlaku platí uvnitř trubice. K předpovědi její hodnoty vně je potřeba vzít v úvahu, že vyzařovací impedance je velmi malá, takže pokles vnitřního tlaku o 40 dB vůči špičkové hodnotě se může ve skutečnosti projevit jako utichnutí akustického vyzařování z trubice.

Druhý typ simulace (viz obr. 4) se zakládal na rychlostních pulzech v trubici. Byly simulovány dva gaussovské pulzy o rozdílné položířce. Zde se dobře ukazuje, že odskok od rezonanční frekvence se projevuje poklesem amplitudy akustického tlaku (viz nejvyšší vrchol, který krátce opouští hodnotu šestého módu). Na asymetrii amplitud i frekvencí

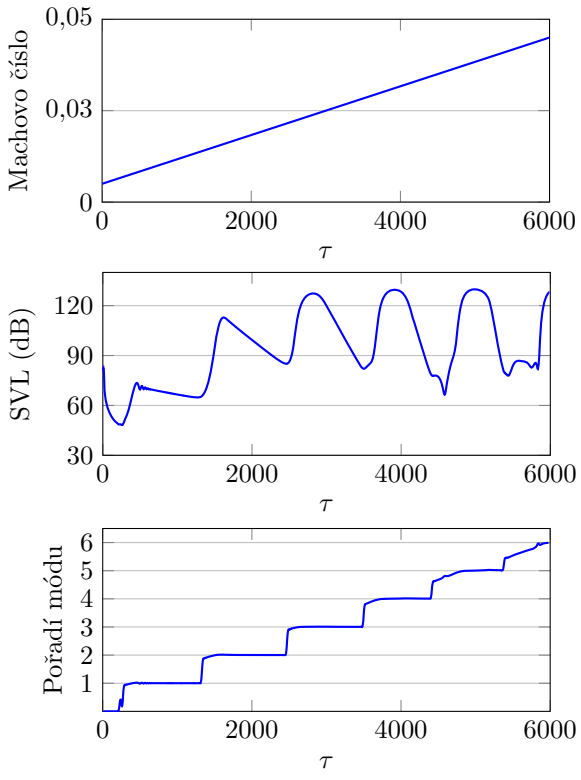

Obrázek 3: Okamžité hladiny akustické rychlosti v ústí trubice a bezrozměrné frekvence systému při rychlostním sweepu

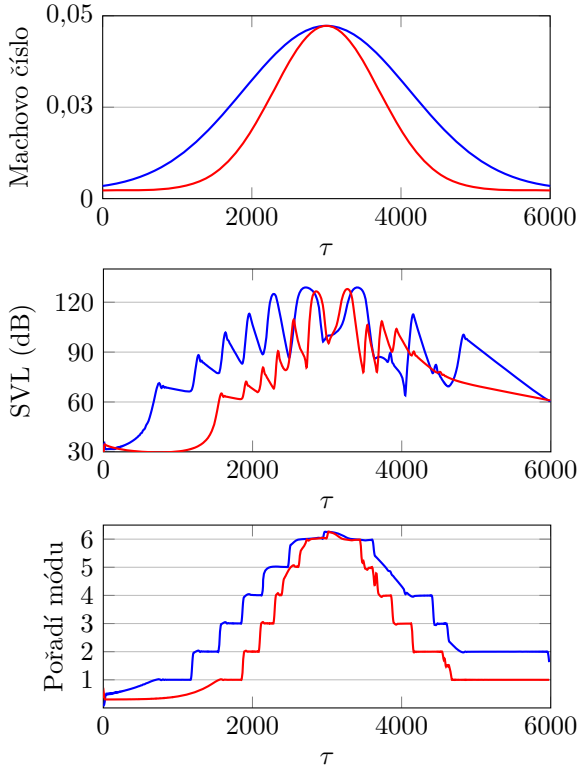

Obrázek 4: Okamžité hladiny akustické rychlosti v ústí trubice a bezrozměrné frekvence systému při systému dvou gaussovských rychlostních pulzů

je patrná hystereze v systému: k přeskoku z nižšího módu na vyšší dochází později než z vyššího na nižší, systém je setrvačný v jednom frekvenčním stavu.

4. Diskuze

V první řadě se zmíníme o limitech tohoto fenomenologického modelu. Teoretické východisko tohoto modelu předpokládá nízká Machova čísla (tzn. uvažuje v intencích nestlačitelného proudění). Při vyšších rychlostech by bylo nutné model upravit a rozšířit (např. uvažovat kompletní Lighthillův tenzor napětí místo zdrojového členu pozůstávajícího z Reynoldsových napětí [8]). Tento případ nicméně není z praktického hlediska příliš významný, protože při transportu tekutin potrubím s vroubkovanou stěnou zpravidla nedochází k jevům transsonického proudění.

Termoviskózní tlumení mimo mezní vrstvu má ve vlnové rovnici velmi malý vliv a je možné ukázat, že i při amplitudách získaných v numerických simulacích by mohlo být zanedbatelné [13]. V modelu je ponecháno kvůli stabilitě, protože amplituda buzeného netlumeného systému v rezonanci by jinak rostla nade všechny meze. Příslušný koeficient je uměle poněkud zvětšen, aby reflektoval i akustické ztráty v mezní vrstvě.

Vliv vroubků na šíření rovinné vlny je v prvním přiblížení možné postihnout zavedením efektivní rychlosti zvuku c_{eff} s ohledem na komplianci vroubků [7]:

$$c_{\text{eff}} = \sqrt{\frac{V_i}{V_{\text{s}}}} c_0 \ , \tag{16}$$

kde V_i je objem segmentu trubice definovaný pomocí jejího (nejmenšího) vnitřního průměru a V_{s} objem celého segmentu. Pro uvažovanou trubici je ovšem c_{eff} konstantní, takže její zavedení místo c_0 nemění kvalitativní charakter uvedených numerických simulací.

Fenomenologický model poskytuje dobrou shodu s experimentálně zjištěným chováním modelovaného systému, kterou je možné pomocí konstant α a B i kvantitativně doladit [1, 7, 6]. Dobře předpovídá znějící základní frekvence a akustický výkon uvnitř trubice, avšak nepostihuje spektrální vlastnosti jak akustického pole v trubici, tak vyzářeného zvuku. Původ druhého aspektu je zřejmý: model neobsahuje vlivy vyzařovací impedance s tím, že její efekt je oproti nelineárnímu tlumení v mezní vrstvě malý. Další odchylku od reálného chování představuje nepřirozeně tvarované zdrojové spektrum. Van der Polův oscilátor poskytuje pro nízké koeficienty nelineárního členu prakticky sinusový signál s malými příspěvky lichých harmonických. Tento charakter reálnému zdroji odpovídá jen v tom ohledu, že základní frekvence má nad zbytkem spektra převahu co do výkonu. „Lichý“ charakter není zdůvodnitelný a ve zdrojovém signálu se obecně vyskytuje relativně silná šumová příměs způsobená chaotickým charakterem turbulentního proudění v okolí vroubků. Pomíjíme toto hledisko s tím, že v případě akustického výzkumu proudění ve vroubkovaných trubicích, který je motivován zejména praktickými konstrukčními hledisky, není poslechová kvalita zvuku rozhodující.

5. Závěr

Předchozí text shrnul teorii zvuku generovaného vířivým prouděním v blízkosti překážek v rozsahu potřebném k vybudování fenomenologického modelu, jehož základní ideou je spojení akustické vlnové rovnice se samobuzenými zdroji van der Polova typu. Výchozí rovnice byly upraveny do modální formulace a s ohledem na obecnost a numerické zpracování byly převedeny do bezrozměrného tvaru.

Numerické simulace ukázaly hlavní kvalitativní znaky zvuku známé z experimentů a analogických systémů [7, 6, 14], tj. nelineární efekt synchronizace budicí a rezonanční frekvence (mode-locking) a hysterezní chování.

Poděkování

Vznik toho článku byl podpořen projektem ČVUT SGS17/130/OHK3/2T/13 a grantem GAČR č. 15-23079S.

Reference

[1] B. Rajavel, M. G. Prasad: Acoustics of corrugated pipes: A review, *Applied Mechanics Reviews*, 65, 2013.

[2] V. Debut, J. Antunes, M. Moreira: A phenomenological model for sound generation in corrugated pipes, In *Proceedings of ISMA*, 2007.

[3] M. Popescu, S. T. Johansen, W. Shyy: Flow-induced acoustics in corrugated pipes, *Commun. Comput. Phys.*, 10, 2011.

[4] M. L. Facchinetti, E. de Langre, F. Biolley: Vortex shedding modeling using diffusive van der pol oscillators, *C. R. Mecanique*, 330:451–456, 2002.

[5] J. Golliard, N. González-Díez, S. Belfroid, G. Nakiboglu, A. Hirschberg: U-RANS model for the prediction of the acoustic sound power generated in a whistling corrugated pipe, In *Volume 4: Fluid-Structure Interaction*. ASME, July 2013.

[6] G. Nakiboglu, S. Belfroid, J. Willems, A. Hirschberg: Whistling behavior of periodic systems: Corrugated pipes and multiple side branch system, *International Journal of Mechanical Sciences*, 52, 2010.

[7] O. Rudenko, G. Nakiboglu, A. Holten, A. Hirschberg: On whistling of pipes with a corrugated segment: Experiment and theory, *Journal of Sound and Vibration*, 332, 2013.

[8] M. S. Howe: *Theory of Vortex Sound*, Cambridge University Press, Cambridge, 2002.

[9] M. S. Howe: The dissipation of sound at an edge, *Journal of Sound and Vibration*, 70(3):407–411, June 1980.

[10] D. Lin, A. Powell: The scattering of hydrodynamic flow into sound by solid bodies – an alternative derivation of Howe's formula, In *Proceedings of ICA*, Seattle, 1998.

[11] D. T. Blackstock: *Fundamentals of Physical Acoustics*, Wiley & Sons, New York, 2000.

[12] T. C. Lieuwen: *Unsteady Combustor Physics*, Cambridge University Press, Cambridge, New York, Melbourne, Madrid, Cape Town, Singapore, Sao Paulo, Delhi, Mexico City, 2012.

[13] L. Menguy, J. Gilbert: Weakly nonlinear gas oscillations in air-filled tubes; solutions and experiments, *Acta Acustica united with Acustica*, 86(5):798–810, 2000.

[14] J. W. Coltman: Jet drive mechanisms in edge tones and organ pipes, *Journal of the Acoustical Society of America*, 60(3):725–733, 1976.

Experimental Estimation of Unknown Parameters of Equivalent Circuits of Low-cost Electret Microphones

Experimentální odhad neznámých parametrů náhradního obvodu low-cost elektretových mikrofonů

Karina Abramova a Petr Honzík

Czech Technical University in Prague, Faculty of Transportation Sciences, Konviktská 20, 110 00 Praha 1, Czech Republic

Properties of low-cost electret microphones can differ significantly among individual items due to the production inaccuracies. This paper presents experimental estimates of some parameters of the equivalent circuit of a low-cost electret microphone which cannot be measured directly, namely the tension of the diaphragm and the equivalent polarization voltage generated by the electret layer. Analysis of the impact of some equivalent circuit parameter variations on the sensitivity of the measured samples has been also carried out (particularly of those that can vary significantly due to the low-cost production). The results show the key role of the equivalent polarization voltage differences, while the differences of the other parameters such as the air gap thickness and the tension of the diaphragm have been found to be much less important.

1. Introduction

The electret microphones (introduced by Sessler in 1962 [1]) have become popular for their properties such as small dimensions, relatively large frequency response, reasonable sensitivity and low price. Moreover, the absence of a need for external polarization voltage presents a practical advantage compared to the classical condenser microphones. Electret microphones are widely used in a large variety of applications such as consumer electronics, or more recently in sensor networks for noise monitoring [2] where the requirement of a high number of sensor nodes raises the need for low-cost solutions (Category 3 in [3]).

When describing the behavior of the microphone, the theoretical model should be chosen at the appropriate level of accuracy. Several models of the condenser microphones can be found in the literature. These models generally take into account the effects of losses originating in the viscous and thermal boundary layers and the strong coupling between the displacement field of the membrane and the acoustic pressure field in the thin fluid layer between the membrane and the fixed electrode, the latter being perforated [4, 5, 6] or not [7, 8]. Although these models are very precise, the simple lumped element model (equivalent circuit) described in several classical textbooks [11, 10, 9] is supposed for this study to be sufficient to provide a good estimate of the microphone behavior in the frequency range up to the frequency of the first resonance with low computational complexity.

Most of the parameters of such a model can usually be determined from the directly measured dimensions of the system and from the material parameters. The accuracy of the model can then be verified by measurements such as laser vibrometry [12, 13] and electrostatic excitation [13, 14, 15, 16] of the membrane movement. However, two parameters, the tension of the membrane and the equivalent polarization voltage produced by the electret layer, cannot be measured directly. In this work, the tension of the membrane has been experimentally determined using the classical method of electrostatic excitation *in vacuo* [15], however, since there is no direct access to the membrane (see section 2), the electrostatic grid has been designed and fabricated specifically for this purpose. The equivalent polarization voltage has been estimated from the measured acoustic pressure sensitivities using a significantly simplified equivalent circuit. Additionally, the analysis of the impact of the membrane tension, the equivalent polarization voltage and the air gap thickness on the sensitivity variations among the measured samples has been performed.

After the introduction, the measured electret microphone is presented in section 2, while the measurements of the acoustic pressure sensitivities and the membrane tension are described in section 3. Section 4 contains a discussion of the impact of certain parameters on the sensitivity variation, and the method to estimate the equivalent polarization voltage is presented. After the conclusion, the lumped element model used for the calculations is introduced in the appendix along with the numerical (FEM) model against which the lumped element model has been tested.

2. Description of the measured microphone

All experiments were performed on a low-cost electret microphone MCA 2500. This microphone consists of a circular membrane of radius R_m, a circular backplate separated from the membrane by a thin air gap of thickness h_g and

Přijato 8. listopadu 2017, akceptováno 20. prosince 2017.

containing three holes of radius R_d regularly azimuthally distributed at the distance h from the border of the electrode which are opened into a back cavity of volume V (see Fig. 1). The aluminium housing of the microphone contains a small opening of radius R_in for acoustic access to a diaphragm. A felt pad covering the input opening was removed prior to calibration. The main dimensional parameters of the microphone are shown in Table 1. The usual value of the density of the membrane material (mylar) of $\rho_\mathrm{m} = 1380\ \mathrm{kg/m^3}$ has been used in the calculations hereafter because of the high incertitude of measurement of the mass and volume of such small samples.

Impedance conversion and signal gain is achieved using an internal JFET transistor placed in the back cavity. The measured volume of the transistor is of order 10^{-10}, which is negligible comparing to the value calculated using the measured cavity dimensions $\pi R_\mathrm{c}^2 h_\mathrm{d}$ given in Table 1. An external preamplifier with the gain of 11 containing the operational amplifier TS971 has been applied on the output of the measured microphone.

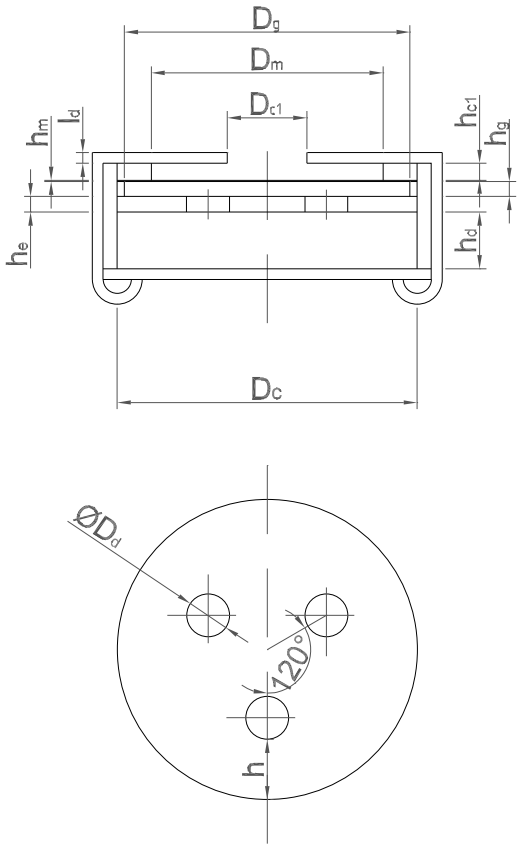

Figure 1: A cross-section view of the electret microphone and a top view of the backplate with holes

3. Experiments and results

In this section, the performed experiments will be described. Eleven samples of the electret microphone randomly selected from three groups purchased during two years (thus most likely from different production series) were used for the measurement.

Table 1: Dimensional parameters of the microphone

Parameter	Symbol	Value
Diaphragm radius	$R_\mathrm{m} = D_\mathrm{m}/2$	$1.975 \cdot 10^{-3}$ m
Diaphragm thickness	h_m	$18 \cdot 10^{-6}$ m
Air gap thickness	h_g	$29.75 \cdot 10^{-6}$ m
Air gap radius	$R_\mathrm{g} = D_\mathrm{g}/2$	$1.975 \cdot 10^{-3}$ m
Radius of the hole in the backplate	$R_\mathrm{d} = D_\mathrm{d}/2$	$0.395 \cdot 10^{-3}$ m
Cavity radius	$R_\mathrm{c} = D_\mathrm{c}/2$	$2.14 \cdot 10^{-3}$ m
Opening radius	$R_{\mathrm{c}_1} = D_{\mathrm{c}_1}/2$	$0.735 \cdot 10^{-3}$ m
Edge distances to hole	h	$1.12 \cdot 10^{-3}$ m
Electrode thickness	h_e	$0.29 \cdot 10^{-3}$ m
Opening length	l_d	$0.20 \cdot 10^{-3}$ m
Input cavity thickness	h_{c_1}	$313 \cdot 10^{-6}$ m
Back cavity thickness	h_d	$1.2 \cdot 10^{-3}$ m
Cavity volume	V_c	$1.856 \cdot 10^{-8}$ m^3

3.1. Acoustic pressure sensitivity

The measurement of the frequency-dependent pressure sensitivity of the microphones will be presented first. The experimental setup (see Fig. 2) is comprised of the measured microphone and the reference 1/4" measurement microphone B&K 4944B, both fitted into a microphone holder of the microphone stand in the quasi-anechoic chamber. The 2-way active studio monitor loudspeaker ESI aktiv 05 is used to generate the exciting acoustic pressure field. The microphones (both supposed to have an omnidirectional directivity pattern) are placed approximately 20 cm from the loudspeaker on its acoustical axis, the distance between them being approximately 1 mm, which assures correct measurement of the acoustic pressure at the input of the measured microphone by the reference microphone in the given frequency range. The signal

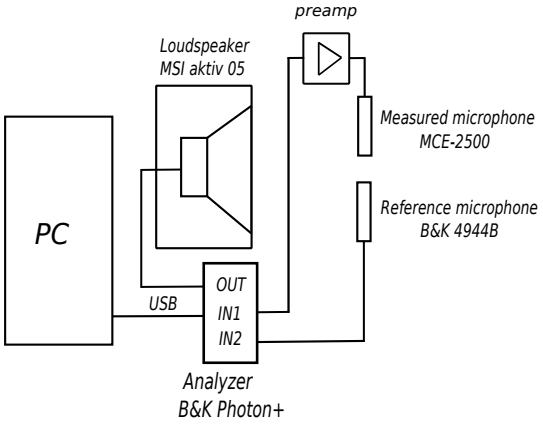

Figure 2: Measuring setup for the measurement of the sensitivity

analyser B&K Photon+ driven by the software B&K RT Pro Photon 7.1 generates the measurement signal (swept sine between 20 Hz and 21 kHz), records the measured signals from both the reference microphone providing the acoustic pressure in Pascals through its known pressure sensitivity (0.853 mV/Pa) and the measured microphone with preamplifier (output voltage signal) and calculates the transfer function between them, which corresponds to the pressure sensitivity of the measured microphone in V/Pa. The electric transfer function of the preamplifier (the same for all microphone samples) has been measured separately in order to remove its influence from the acoustic pressure sensitivity measurements.

The measured pressure sensitivities are depicted in Fig. 3. Table 2 shows the values of the pressure sensitivities at the frequency of 1 kHz along with the corresponding values in dB, where the reference is 1 V/Pa. The last column in Table 2 presents the height of the sensitivity peak calculated as the difference between the sensitivity at 1 kHz and at the peak of the sensitivity curve in dB giving an idea about the damping in the system. It is clearly visible that the pressure sensitivity values of the measured microphone samples differ in a relatively wide range (from 3.8 mV/Pa to 16.4 mV/Pa which represents the range of 12.7 dB). However, the position of the first resonance of the whole system, which determinates the microphone bandwidth, seems to be similar for all measured samples of the microphone (around 10 kHz). The height of the sensitivity peak ranges from 5 dB (sample No. 1) to 8.5 dB (sample No. 6), but ten of eleven samples present a value not exceeding 6.8 dB, which shows only a relatively small difference of the damping between the samples.

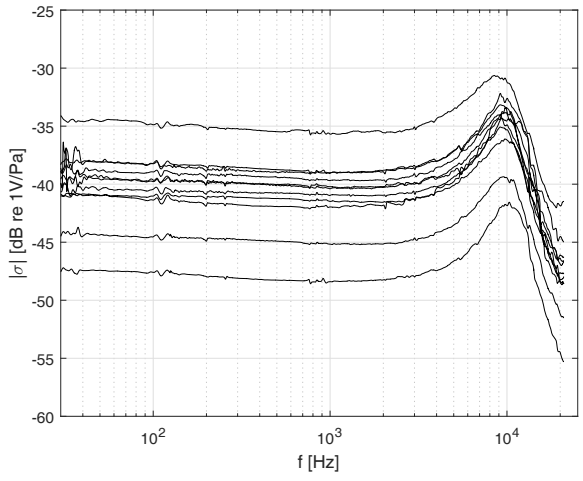

Figure 3: Measured frequency responses of the microphones in free-field

3.2. Tension of the membrane

The tension of the membrane is an important parameter of the equivalent circuit which cannot be measured directly;

Table 2: The measured pressure sensitivities and heights of the resonance peaks

No.	$\sigma_{1\mathrm{kHz}}$(dB)	mV/Pa	Δ (dB)
1	−35.6	16.4	5.0
2	−39.0	11.1	6.8
3	−40.9	8.9	5.8
4	−41.4	8.4	5.3
5	−40.3	9.5	6.4
6	−41.9	7.9	8.5
7	−39.0	11.2	5.8
8	−40.2	9.7	5.8
9	−45.1	5.5	5.8
10	−48.3	3.8	6.8
11	−39.6	10.3	5.8

however, it can be calculated from the measured frequency of the first mode of the membrane. In order to eliminate the impact of all acoustical elements except the membrane, the measurement of the resonance frequency has to be performed in a vacuum chamber. The well-known method using the electrostatic grid to excite the motion of the membrane is applied in the present study.

Since the eigenfrequencies f_n $(n = 1, 2, \dots)$ of the membrane modes *in vacuo* are given by the equation $\mathrm{J}_0(2\pi f_n/\sqrt{T/m_\mathrm{s}}) = 0$ [9, 10], $m_\mathrm{s} = \rho_\mathrm{m} h_\mathrm{m}$ being the surface density of the membrane, $\mathrm{J}_0(x)$ being the 0-th order Bessel function of the first kind, the tension T of the membrane can be calculated from the measured first eigenfrequency $f_\mathrm{res} = f_1$ as follows

$$T = m_\mathrm{s} \left(\frac{2\pi f_\mathrm{res} R_\mathrm{m}}{j_1} \right)^2 , \qquad (1)$$

where $j_1 \approx 2.4048$ is the first solution of the equation $\mathrm{J}_0(j_n) = 0$.

Unlike the classical condenser microphones, the electret microphone considered here has no direct access to the membrane, hence the classical electrostatic grid [13, 14] cannot be used. For this reason, a special electrostatic grid has been fabricated. The classical printed circuit board with a copper-plated via hole was milled from one side around the via hole in order to form a small cylindrical tip with the via hole inside, the radius of the tip being slightly smaller than the radius of the microphone's input opening. The tip has been put into the microphone's input opening in such a manner that the copper surface on the tip is sufficiently close to the membrane and electrically connected to the outer side of the printed circuit board, so that the electrostatic excitation of the membrane can be performed (see Fig. 4). The rest of the Figure 4 shows the classical measurement setup used for the electrostatic calibration [13], except for the chamber where the microphone with its preamplifier and the electrostatic grid is placed in this case. Concerning the static pressure in the vacuum chamber, the lower pressure limit of the vacuum system used here is slightly below 1 Pa. The variations of the first eigenfrequency of the membrane for the static pressures below

1 Pa are assumed to be negligible. The polarization voltage applied to the grid is equal to $U_G = 100$ V. Similarly to the measurement of the acoustic pressure sensitivity, the swept sine is used as the exciting signal, however here, only the frequency dependent voltage level at the output of the microphone preamplifier is traced by the analyser.

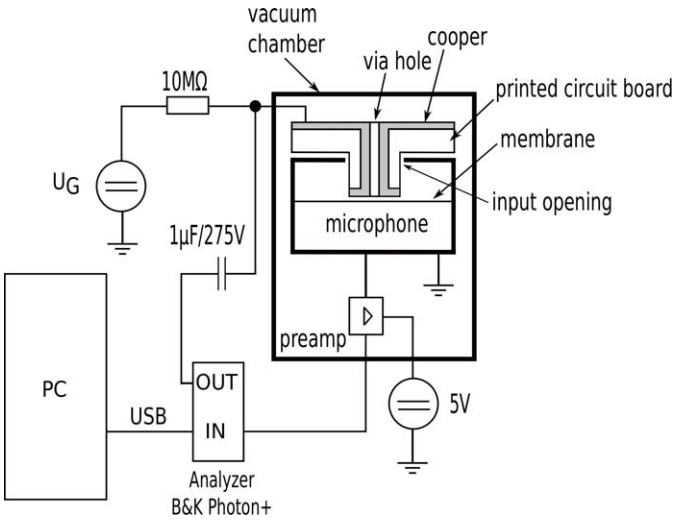

Figure 4: Measurement setup for the measurement in the vacuum

The results of the measurements are shown in Fig. 5. The maxima of the microphone output levels correspond to the first eigenfrequencies of the membranes. Table 3 summarizes the static pressures P_0 achieved during the measurements, the values of the measured eigenfrequencies f_{res} and the membrane tensions T for all microphone samples. The measured eigenfrequencies of the membranes range from 11.595 kHz to 12.364 kHz, which leads to the tensions of the membranes ranging from 88.9 N/m to 101.1 N/m.

Table 3: The measured resonance frequencies and tensions

No.	P_0 (Pa)	f_{res} (kHz)	T (N/m)
1	0.62	11.946	94.4
2	0.59	12.364	101.1
3	0.60	11.879	93.3
4	0.64	11.681	90.2
5	0.46	11.813	92.3
6	0.60	11.665	90.0
7	0.28	11.662	89.9
8	0.47	12.154	97.7
9	0.62	11.737	91.1
10	0.59	11.595	88.9
11	0.60	12.222	98.7

4. Analysis of the results and discussion

In this section, the results of the measurements will be analysed in order to i) find the parameter of the equivalent circuit describing the huge variation of the acoustic pressure sensitivities among the samples of the electret microphones and ii) estimate the unknown equivalent polarization voltage U_0 which cannot be measured directly.

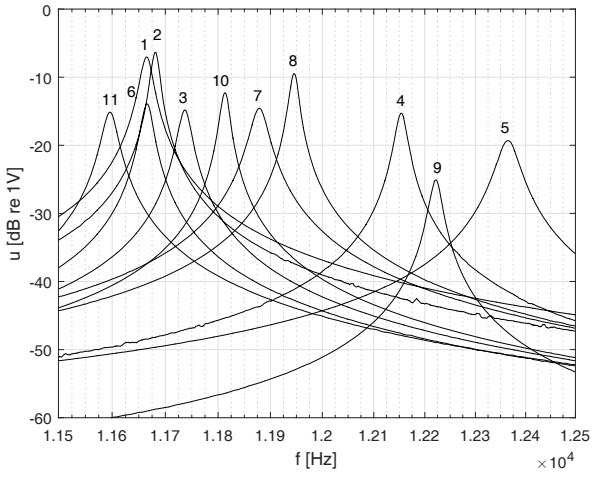

Figure 5: The first resonance frequency peaks in the vacuum

It should first be noted that the parameters of the air (see Tab. 7 in the Appendix) are supposed to be constant and do not influence the variation of the acoustic pressure sensitivities. Beyond these parameters, the variation of all geometrical parameters given in Table 1, membrane density ρ_{m}, membrane tension T and equivalent polarization voltage U_0 can theoretically influence the acoustic pressure sensitivity of the microphone. The effect of the variation of the membrane tension T is analysed in the subsection 4.1, which contains the influence of the others parameters of the membrane, namely its thickness h_{m}, radius R_{m} and density ρ_{m} related with the membrane tension (see eq. 1). Concerning the dimensions of the air-filled parts of the microphone, only the airgap thickness h_{g} is supposed to be sufficiently small to vary significantly due to the production inaccuracies. The influence of the airgap thickness h_{g} on the acoustic pressure sensitivity is analysed in the subsection 4.2. The subsection 4.3 presents a method to obtain a rough estimate of the equivalent polarization voltage U_0.

In order to compare the results of the model of the microphone for varying parameters T and h_{g} while one parameter of the model – the polarization voltage U_0 – is not known, the adimensional sensitivity [8]

$$\sigma_{\mathrm{adim}} = -\frac{\bar{\xi}}{h_{\mathrm{g}}} = \sigma \frac{p_{\mathrm{inc}}}{U_0}, \tag{2}$$

is used in the subsections 4.1 and 4.2, the reference incident pressure being 1 Pa.

4.1. The influence of the membrane tension on the acoustic pressure sensitivity

The measured membrane tensions T present certain variations among the measured microphone samples (see section 3.2) resulting in the variation of the pressure sensitivities of the microphones. The adimensional sensitivities calculated using the slumped-element model (see Appendix) with the measured membrane tensions used as model inputs are calculated here, the other parameters of the model being fixed according to Tables 1 and 7. Table 4 presents the adimensional sensitivities at 1 kHz for the maximal and minimal membrane tension, showing that the variation of the measured tensions (from 88.9 N/m to 101.1 N/m) cannot cause such a huge variation of acoustic pressure sensitivities measured in the section 3.1 (12.7 dB), the modelled sensitivities resulting here to the range of 1.3 dB.

Table 4: Dependence of the adimensional sensitivity on the membrane tension calculated from microphone model

T (N/m)	σ_{adim}(1 kHz) (dB)
101.1	−79.2
88.9	−78.5

4.2. The influence of the the air gap thickness on the acoustic pressure sensitivity

Concerning the impact of the airgap thickness h_{g} variation on the frequency-dependent acoustic pressure sensitivity, it should be pointed out that there are two main areas of the sensitivity curve influenced by this parameter: i) the height of the sensitivity peak in the higher frequency range given by the damping in the system and ii) the flat part in the lower and middle frequency range. Regarding the model, the real part of the airgap impedance (see eq. A.2 in the Appendix), which models the damping in the system, contains h_{g}^3 in the denominator, which makes the variation of this geometrical parameter relatively important. However, equation (A.5) shows only $1/h_{\mathrm{g}}$ dependence of the acoustic pressure sensitivity for constant mean displacement of the membrane in the lower and middle frequency range. As presented in Table 5, the change of h_{g} from 30 μm to 35 μm (the other parameters being given in the Tables 1 and 7, the membrane tension being $T = 100$ N/m) causes the change in the height of the sensitivity peak which is similar to the range of the measured variation, while the adimensional sensitivity at 1 kHz decreases only by 1.3 dB. This shows that the measured variation of the acoustic pressure sensitivity of 12.7 dB, while the measured height of the sensitivity ranges from 5 dB to 8.5 dB, cannot be caused by the variation in the airgap thickness.

Since the impact of the membrane tension and the airgap thickness on the acoustic pressure sensitivity given by the model is relatively low, proceeding by elimination, it was concluded that the parameter responsible for the variation of the measured acoustic pressure sensitivity is the equivalent polarization voltage U_0.

Table 5: Dependence of the adimensional sensitivity and the height of the sensitivity peak on the gap thickness calculated from microphone model

h_{g} (m)	ΔdB (dB)	σ_{adim}(1 kHz) (dB)
$30 \cdot 10^{-6}$	4.6	−79.2
$35 \cdot 10^{-6}$	8.2	−80.5

4.3. Estimation of the equivalent polarization voltage

The polarization voltage applied between the membrane and the backplate in the classical condenser microphones is replaced by the electret layer, providing the electric charge for the electret microphone. The parameter of the equivalent circuit, here called U_0, corresponds to the equivalent polarization voltage that would cause the same behavior of the electret microphone if there were no electret layer. This parameter cannot be measured directly, yet a rough estimate of U_0 can be obtained from the significantly reduced equivalent circuit at low frequencies.

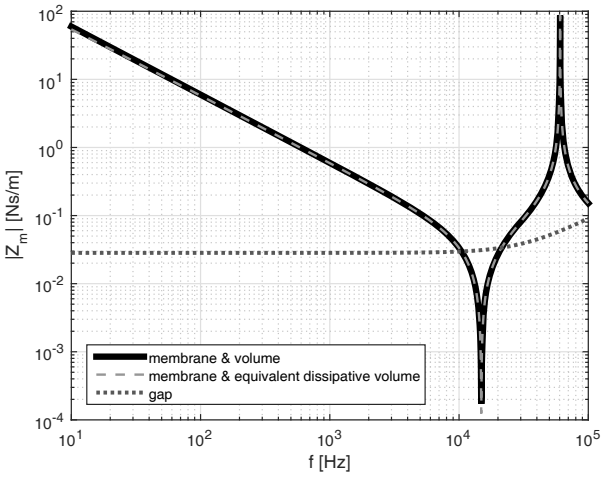

Figure 6: Mechanical impedances of parts of the complete equivalent circuit

Figure 6 shows a comparison of absolute values of mechanical impedance in some parts of the complete equivalent circuit (from Fig. 9). It is clearly visible that the impedance of the airgap and the holes in the backplate is much lower in terms of absolute value than the impedance of the membrane and the back cavity at low frequencies (more than 100 times at 100 Hz) and can be neglected in order to form a low-frequency equivalent circuit. Furthermore, when omitting the mass of the membrane, the change of the value of the impedance at low frequencies is negligible, thus the significantly reduced equivalent circuit

containing only the quasi-static compliance of the membrane and the mechanical compliance of the backing cavity (Fig. 7) can be used at very low frequencies. Note, that the effects of the thermal losses in the backing cavity cannot be neglected at very low frequencies. In order to improve the model behavior in this frequency range by taking into account these effects, the volume of the cavity V_c in the usual adiabatic approximation of the cavity compliance (see eq. (A.4)) is replaced here by the complex equivalent volume [10]

$$V_\mathrm{cplx} = V_\mathrm{c}\left(1 + (1-\mathrm{j})(\gamma-1)S_\mathrm{c}\frac{\sqrt{c\frac{l_\mathrm{h}}{\omega}}}{V_\mathrm{c}\sqrt{2}}\right), \qquad (3)$$

where $S_\mathrm{c} = 2\pi R_\mathrm{m}\cdot(R_\mathrm{m}+h_\mathrm{d})$ is the surface of the cavity, $l_\mathrm{h} = \lambda_\mathrm{h}/(\rho_0\, c\, C_p)$ is the characteristic thermal length, the other parameters of the fluid being given in the Table 7. In using the relations for the velocity of the membrane $v_\mathrm{m} = \mathrm{j}\omega\bar{\xi}$ and for the input mechanical impedance of the microphone $Z_\mathrm{in} = p_\mathrm{inc}S_\mathrm{m}/v_\mathrm{m}$, the acoustic pressure sensitivity (eq. (A.5)) can be expressed as

$$\sigma = -U_0\frac{S_\mathrm{m}}{\mathrm{j}\omega Z_\mathrm{in}h_\mathrm{g}}. \qquad (4)$$

Since the input impedance at low frequencies is given by the equivalent circuit from the Figure 7 as $Z_\mathrm{in} = 1/(\mathrm{j}\omega(C_\infty + C_{V_\mathrm{m}}))$, the rough estimate of the equivalent polarization voltage can be calculated from the value of the measured acoustic pressure sensitivity σ_meas (see subsection 3.1) at low frequency (here 100 Hz) as follows

$$U_0 = \left|\frac{h_\mathrm{g}\,\sigma_\mathrm{meas}(100\,\mathrm{Hz})}{S_\mathrm{m}(C_\infty + C_{V_\mathrm{m}})}\right|. \qquad (5)$$

The calculated estimates of the equivalent polarization voltages of all measured samples of the electret microphone are shown in Table 6. Figure 8 depicts the comparison between the measured and the calculated acoustic pressure sensitivity of three microphone samples, one for the lowest and one for the highest sensitivity and one for the middle one. A good agreement between the theoretical results obtained from the full equivalent circuit (see Appendix) with the estimated parameters and the measured sensitivity curves can be observed. The slight shift in the resonance frequency can be caused by the fact that

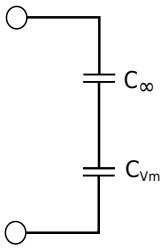

Figure 7: The simplified low-frequency equivalent circuit

Table 6: The estimated equivalent polarization voltages

No.	U_0 (V)	No.	U_0 (V)
1	147.7	7	100.3
2	100.9	8	84.1
3	78.1	9	48.7
4	72.9	10	34.2
5	85.2	11	92.5
6	70.0		

the density of the membrane has not been measured (the usual value has been used – see section 2 for explication). The damping of the system (according to the height of the resonance peak) seems to be predicted correctly for the sample No. 1 and slightly overestimated for the other two samples shown in Figure 8, just as in the case of the comparison of the lumped element model with the FEM results (see the end of Appendix).

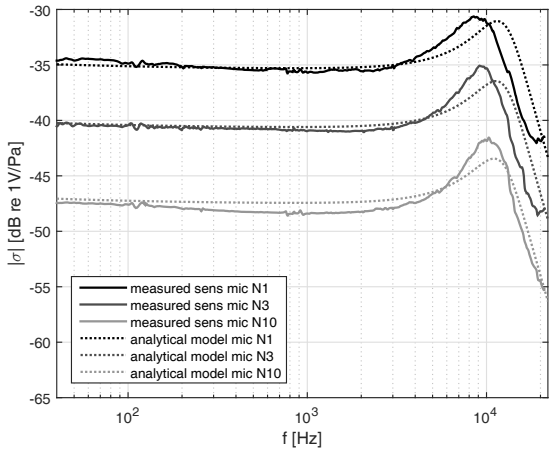

Figure 8: The measured and the calculated acoustic pressure sensitivities of three microphone samples

5. Conclusion

Two parameters of the equivalent circuit of the low-cost electret microphone which cannot be determined from the microphone dimensions and material constants or measured directly, the membrane tension and the equivalent polarization voltage, have been estimated. The impact of the these two parameters on the sensitivity variation among the measured samples has been analysed. The results show that the sensitivity variation strongly depends upon the variation of the equivalent polarization voltage while the effect of the air gap thickness and the tension of the diaphragm is found to be much less important. A good agreement between the measured frequency responses of the measured microphones and the theoretical sensitivity curves calculated using the equivalent circuit with the estimated parameters has been observed.

Acknowledgement

This work was supported by the Grant Agency of the Czech Technical University in Prague, grant No. SGS15/226/OHK2/3T/16.

Appendix – The equivalent circuit of the microphone

The classical lumped-element model [9, 10, 11] of the microphone (with some particularities described in this section) is considered in this section. The equivalent circuit shown in Figure 9 consists of the acoustic, mechanic and electric parts, which are presented hereafter. Note that the input opening and the input cavity are omitted in the equivalent circuit, because the effect of this system is supposed to be negligible in the frequency range of interest (small dimensions lead to the resonant frequency above the first eigenfrequency of the membrane).

The link between the acoustic and mechanical domain is modelled by the mechano-acoustic transformer with the ratio $1 : S_\mathrm{m}$ at the input of the model, $S_\mathrm{m} = \pi R_\mathrm{m}^2$ representing the diaphragm area, p_inc is the incident acoustic pressure. The second transformer represents the coupling between the electric and mechanical domain with the ratio $1 : k_\mathrm{b}$, where $k_\mathrm{b} = C_0 U_0 / h_\mathrm{g}$ is the transducer factor, $C_0 = \varepsilon_0 S_\mathrm{m} / h_\mathrm{g}$ being the static capacitance of the microphone (the effect of the holes in the back electrode on the microphone static capacitance is neglected because of their small dimensions, along with the edge effect of the electrostatic field near the holes). Note that since the transducer is supposed to operate with constant charge, the negative compliance $-c_\mathrm{n} = -C_0 / k_\mathrm{b}^2$ (which should be theoretically present in the equivalent circuit) can be neglected [9]. The mechanical domain between the two transformers mentioned above consists of the components representing the membrane and the air-filled acoustic elements behind the membrane (transformed to the mechanical domain).

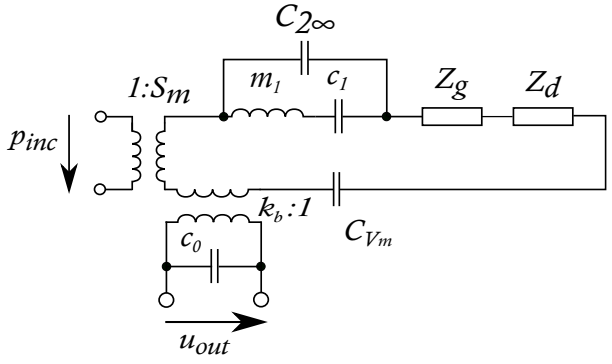

Figure 9: Complete equivalent circuit of the microphone

The membrane behavior is described by the components

$$\begin{aligned} c_1 &= \frac{4}{j_1^4 \pi T}, \\ m_1 &= \frac{j_1^2}{4} m_\mathrm{s} S_\mathrm{m}, \\ C_{2\infty} &= C_\infty - c_1, \end{aligned} \tag{A.1}$$

where the mechanical compliance c_1 and the mass m_1 determine the first membrane eigenfrequency (see section 3.2 for the meaning of j_1), $C_\infty = 1/8\pi T$ is the quasistatic compliance of the membrane and $C_{2\infty}$ provides a correction of the low-frequency behavior.

The mechanical impedance of the air gap between the membrane and the backplate with holes of radius R_d can be calculated as follows [9, 17]

$$Z_\mathrm{g} = N \left(\frac{6\mu\pi X_0^4 \beta}{h_\mathrm{g}^3} + \mathrm{j}\omega \frac{\rho_0 \pi X_0^4 \beta}{2 h_\mathrm{g}} \right), \tag{A.2}$$

where N is the number of holes in the backplate, herein $N = 3$, $X_0 = \sqrt{S_\mathrm{m}/(N\pi)}$ is an equivalent circular region collecting the air flow from each hole and

$$\beta = \ln \frac{X_0}{R_\mathrm{d}} - \frac{3}{4} + \frac{R_\mathrm{d}^2}{X_0} - \frac{1}{2} \frac{R_\mathrm{d}^4}{X_0^4}.$$

The holes are modelled by the mechanical impedance

$$\begin{aligned} Z_\mathrm{d} = & \frac{S_\mathrm{m}^2}{N} \left[\frac{8 h_\mathrm{e} \mu}{\pi R_\mathrm{d}^4} + \mathrm{j}\omega \frac{4 \rho_0 h_\mathrm{e}}{3\pi R_\mathrm{d}^2} + \right. \\ & \left. 2\mathrm{j}\,\omega \frac{\rho_0}{X_0} \left(0.26164 - 0.353\,\alpha + 0.0809\,\alpha^3 \right) \right]. \end{aligned} \tag{A.3}$$

where the first two terms in the bracket represent the resistance and the mass of the holes [9] and the third term with $\alpha = R_\mathrm{d}/X_0$ is the added mass modelling the influence of the sharp edges of the holes [18]. Note that the section of the holes in the backplate $S_\mathrm{h} = \pi R_\mathrm{d}^2$ is supposed to be much smaller than the surface of the membrane S_m.

The mechanical compliance of the back cavity is given by the classical expression

$$C_{V_\mathrm{m}} = \frac{V_\mathrm{c}}{\rho_0 c^2 S_\mathrm{m}^2}. \tag{A.4}$$

where the cavity volume V_c can be replaced by the complex equivalent volume (see eq. (3) in section 4.3).

The pressure sensitivity of the microphone, defined as the ratio of the output voltage and the incident pressure p_inc can be expressed using the classical formula

$$\sigma = -U_0 \frac{\bar{\xi}}{p_\mathrm{inc} h_\mathrm{g}}, \tag{A.5}$$

where $\bar{\xi}$ is the mean value of the membrane displacement over the back electrode surface. The pressure sensitivity derived from the equivalent circuit is usually presented in the following form [9]

$$\sigma = \frac{k_\mathrm{b} S_\mathrm{m}}{k_\mathrm{b}^2 + \mathrm{j}\omega C_0 Z_\mathrm{total}}, \tag{A.6}$$

where Z_{total} is the mechanical impedance given by the combination of all the components in the mechanical domain of the equivalent circuit. The term k_{b}^2 is negligible compared to the other terms in the denominator and can be omitted, which is equivalent to neglecting the negative compliance mentioned above [9].

The lumped-element model described above has been verified by the numerical FEM model using the software Comsol Multiphysics, version 5.2. Although this software optionally contains a module that, enables to take into account the effects of the viscous and thermal boundary layers through a formulation simultaneously calculating the acoustic particle velocity, the temperature variation and the acoustic pressure [19, 20], the alternative formulation calculating only the particle velocity and the temperature variation [21] (thus reducing the number of degrees of freedom) has been used here.

The comparison between the results obtained from the equivalent circuit and from the numerical model for the parameters of air given in Table 7, the dimensions of the microphone given in Table 1 and for $T = 100$ N/m and $U_0 = 100$ V is shown in Figure 10. A very good agreement can be observed in the frequency range of interest (up to the frequency of the first resonance), the damping of the system being slightly overestimated by the lumped-element model. Since the boundary layers regions have to be meshed correctly in the FEM model, the appropriate 3D mesh leaded to 989 356 degrees of freedom (even though the meshed geometry contained only 1/6 of the microphone, the rest being symmetric), the whole calculation took 8 hours and 39.5 minutes (approximately 12 minutes per one frequency point) on the eight-core Intel Xeon processor at 2.4 GHz and 84 GB of RAM has been used. This shows clearly the advantage of the equivalent circuit method, where the result is obtained immediately with reasonable precision and much lower computational costs.

Table 7: Parameters of the air

Parameter	Symbol	Value/Unit
Adiabatic sound speed	c	345.9 $\text{m}\cdot\text{s}^{-1}$
Air density	ρ_0	1.18 $\text{kg}\cdot\text{m}^{-3}$
Shear dynamic viscosity	μ	$1.83\cdot10^{-5}$ $\text{Pa}\cdot\text{s}$
Permittivity	ε_0	$8.8542\cdot10^{-12}$ $\text{F}\cdot\text{m}^{-1}$
Thermal conductivity	λ_{h}	$24.4\cdot10^{-3}$ $\text{W}/(\text{m}\cdot\text{K})$
Specific heat coefficient at constant pressure per unit of mass	C_p	1010 $\text{J}/(\text{kg}\cdot\text{K})$
Ratio of specific heats	γ	1.4
Static pressure	P_0	101.325 Pa
Static temperature	T_0	293.15 K

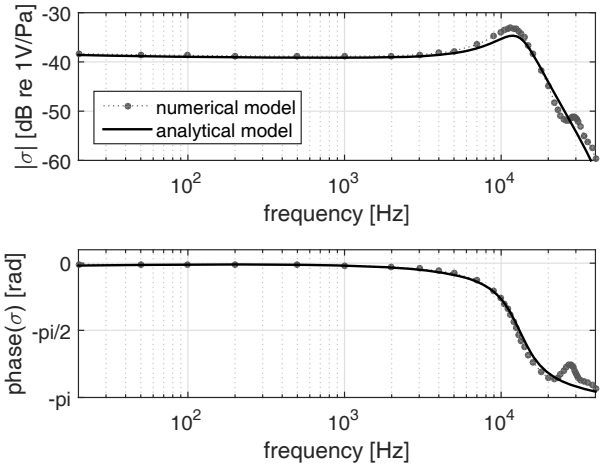

Figure 10: The comparison between the acoustic pressure sensitivity obtained from the equivalent circuit (full line) and the one obtained from FEM simulations (dashed line with circular marks); upper figure: module of the sensitivity, lower figure: phase of the sensitivity

References

[1] Sessler, G. M., West, J. E.: Self-biased Condenser Microphone with High Capacitance, *J. Acoust. Soc. Am.* **34**(11), 1787–1788, (1962).

[2] Brynda, P., Kopřiva, J., Horák, M.: Trafficsensnet Sensor Network for Measuring Emissions from Transportation. In: Procedia Engineering Special Issue Eurosensors 2015, Eurosensors 2015, Freiburg, 6.–9. 9. 2015, Oxford: Elsevier Ltd, 902-907, (2015), ISSN 1877-7058.

[3] Wessels, P. W., Basten, T. G. H.: Design aspects of acoustic sensor networks for environmental noise monitoring, *Applied Acoustics*, 110, 227–234, (2016).

[4] Zuckerwar, A. J.: Theoretical response of condenser microphones, *J. Acoust. Soc. Am.*, **64**(5), 1278–1285, (1978).

[5] Lavergne, T., Durand, S., Bruneau, M., Joly, N., Rodrigues, D.: Dynamic behavior of the circular membrane of an electrostatic microphone: Effect of holes in the backing electrode, *J. Acoust. Soc. Am.*, **128**(6), 3459–3477, (2010).

[6] Lavergne, T., Durand, S., Joly, N., Bruneau, M.: Analytical Modeling of Electrostatic Transducers in Gases: Behavior of Their Membrane and Sensitivity, *Acta Acust. united Ac.*, **100**, 440–447, (2014).

[7] Bruneau, M., Bruneau, A.-M., Škvor, Z., Lotton, P.: An equivalent network modelling the strong coupling between a vibrating membrane and a fluid film, *Acta Acust. united Ac.*, **2**, 223–232, (1994).

[8] Le Van Suu, T., Durand, S., Bruneau, M.: On the modelling of clamped plates loaded by a squeeze fluid film: application to miniaturised sensors, *Acta Acust. united Ac.*, **96**(5), 923–935, (2010).

[9] Škvor, Z.: *Vibrating Systems and their Equivalent Circuits*, Elsevier, Amsterdam, (1991).

[10] Bruneau, M., Scelo, T.: (translator and contributor) Fundamentals of Acoustics, ISTE, London, (2006).

[11] Beranek, L. L., Mellow, V. T.: *Acoustics: Sound Fields and Transducers*, Elsevier, UK, USA, (2012).

[12] Barrera-Figueroa, S., Rasmussen, K., Jacobsen, F.: Hybrid method for determining the parameters of condenser microphones from measured membrane velocities and numerical calculations, *J. Acoust. Soc. Am.*, **126**, 1788–1795, (2009).

[13] Honzík, P., Podkovskiy, A., Durand, S., Joly, N.: Experimental investigation on the electrostatic receiver with small-sized backing electrode, *Forum Acusticum 2014*, Krakow, (2014).

[14] International Electrotechnical Commission IEC 61094-6, Measurement microphones, part 6: Electrostatic actuators for determination of frequency response, (2004).

[15] Guianvarch, C., Gavioso, R. M., Benedetto, G., Pitre, L., Bruneau, M.: Characterization of condenser microphones under different environmental conditions for accurate speed of sound measurements with acoustic resonators, *Rev. Sci. Instrum. 80*, 074901, (2009).

[16] Jarvis, D. R.: The accuracy of the electrostatic actuator method of determining the frequency response of condenser microphones, *J. Sound Vib.*, 123, 63–70, (1988).

[17] Škvor, Z.: On the Acoustical Resistance Due to Viscous Losses in the Air Gap of Electrostatic Transducers, *Acustica*, **19**(5), 295–299, (1967).

[18] Kergomard, J., Garcia, A.: Simple discontinuities in acoustic waveguides at low frequencies: critical analysis and formulae, *J. Sound Vib.*, **114**(3), 465–479, (1987).

[19] Kampinga, W. R., Wijnant, Y. H., de Boer, A.: An Efficient Finite Element Model for Viscothermal Acoustics, *Acta Acust. united Ac.*, **97**, 618–631, (2011).

[20] Jensen, M. J. H., Olsen E. S.: Virtual prototyping of condenser microphones using the finite element method for detailed electric, mechanic, and acoustic characterization, *Proceedings of Meetings on Acoustics*, vol. 19, pp. 030039, (2013).

[21] Joly, N.: Finite Element Modeling of Thermoviscous Acoustics on Adapted Anisotropic Meshes: Implementation of the Particle Velocity and Temperature Variation, *Acta Acust. united Ac.*, **96**(1), 102–114, (2010).

The Arrangement of Noiseless Sound and Vibration High Speed Camera Recordings

Zařízení pro bezšumový záznam zvuku a vibrací vysokorychlostní kamerou

Milan Guštar a Zdeněk Otčenášek

Music and Dance Faculty, Academy of Performing Arts in Prague Prague, Czech Republic
zdenek.otcenasek@hamu.cz

The high-speed camera recordings require the use of intense illumination. When the vibration of a sound source element and sound needs to be recorded simultaneously with a high-speed camera and a microphone, the audio recording is affected by the noise of the cooling fans of the used devices e.g. powerful lamps. Noiseless recording conditions, however, are essential in the usual sound and vibration causality studies. The paper presents a possibility of noise elimination with the fans-off device used in the research of the causal relation between violin string vibration and tone sound. The high-speed camera is operating at 60 kfps which needs the illumination with high-power 1 kW spotlight. The device switches all cooling fans off for the necessary time periods prior to the measurement and thus ensures the noiseless operation of the apparatus during the audio/video recording. After the recording, the device automatically switches the fans on to ensure the proper equipment cooling. The device provides the audio/video triggering and synchronization as well. An example of the result is presented; for more about discovered causality see in Full Paper link at: `http://viennatalk2015.mdw.ac.at/?page_id=13002&pap=36`.

1. Applicability

The presented fans-off device application in the sound and vibration measurements serves as an example of a controlled measuring arrangement. The described hardware and software solution is applicable not only in the case of a noiseless sound and vibration high-speed camera recording but also in various situations where a sequence of control steps with appropriately adjusted timing is required. Hence the proposed device can be used for the on/off timing of electric actuators, sensors and other devices, for the generation of excitation or synchronization signals, etc.

2. Introduction

In the research of mechanical vibration, it is often necessary to perform acoustic measurements or to record acoustical signals produced by the objects under examination. The measurement hardware itself is often a source of unwanted sound or noise interfering with the acoustic signal to be measured or recorded. The most common sources of the noise are cooling systems of recording or measuring devices (computers, high-speed cameras, disk arrays, etc.), light sources (high-power lamps, lasers, etc.), and other devices.

Fan noise decreases the signal-to-noise ratio, degrades the recording quality and can even make the recording or measurement of quiet sounds impossible. The noise can reduce the precision or render impossible the objective sound analysis as well as the subjective listening tests.

Noise elimination by means of absorbing acoustic panels may not be sufficient, since the panel placement can have a negative impact on the implementation of experiments or on the frequency characteristics of microphones, transducers and other sensing elements [1, 2].

Signal filtering or the use of noise reduction algorithms usually significantly affects the useful signal components resulting in the bias of the results or even their complete degradation. When a high number of frames per second is used in high-speed camera recordings, a high-power lamp is necessary, but the recording time is relatively short due to the GB size of video records. It is possible to switch off the device fans for this short time and then to obtain the noiseless sound recording condition.

3. Noise elimination solution

The proposed Fans-off device provides very efficient short-time noise cancellation both for one-time as well as repeated noiseless sound recordings or measurements. The device turns off all noise-producing cooling fans for the time span necessary to perform the measurements (usually in the time spans of up to tens of seconds) and generates the required start and stop triggering signals e.g. for the camera. It provides the synchronization of all turn-off sequence steps with the measurement to ensure the shortest possible operation without active cooling and to safeguard a sufficiently long break before the next measurement to avoid exceeding the permissible operating temperature of all individual components of the measurement system.

Přijato 4. listopadu 2016, akceptováno 18. října 2017.

The operator can adjust the timing and other parameters of the proper fans-off sequence according to experimentally measured values for the incorporated equipment with respect to the individual fans' deceleration times. The optimized fans-off sequence minimizes its operation time without the active cooling and together with the sufficient fans-on time lags between consecutive measurement steps ensure the sufficient cooling of all devices in the measurement set-up.

For the device design, a microcontroller-based solution was chosen because the selected microcontroller (MCU) provides all building blocks required for the purpose, and MCUs allow rapid and easy development of various embedded systems, simple specialised controllers, etc.

The heart of the Fans-off device is the microcontroller from the Atmel AVR family (ATtiny2313, [3]). This electronic device contains a central processor unit, memories and all other blocks of a self-contained microcomputer on a chip. The MCU chip is equipped with various communication interfaces, ports, timers, analogue comparator, A/D converter and other peripherals which allow easy links to the controlled system. Available development tools enable efficient software build-up. An In-system programming (ISP) port serves for fast software debugging and updating.

In the presented case, the AVR MCU serves for the timing and the generation of all signals during the sequences of fans switching off and on. The Fans-off device electronic circuit schematic diagram is in Fig. 1.

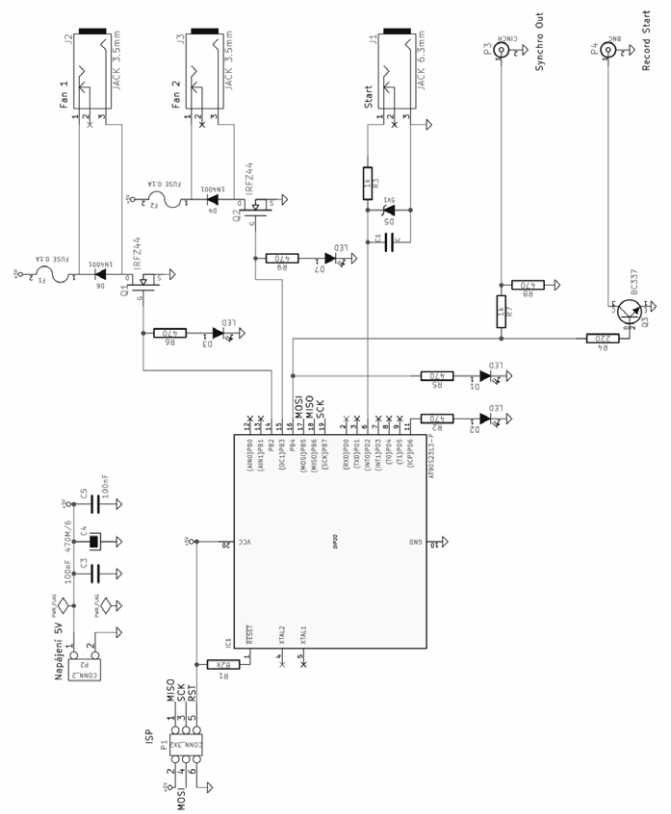

Figure 1: The Fans-off device schematics

The fans are switched off using relays with a break contact embedded in the controlled devices (the camera and the light source). The relays are connected to the Fans-off device by means of connectors. Without the connected Fans-off device, the relays do not affect the fans function and devices can be used independently in the usual manner.

The measurement sequence is initiated by the Start synchronization impulse in the form of the TTL signal fed to the Trigger Input connected with the INT0 MCU pin. Alternatively, an electrical switch can be used. Consequently, the controlled devices are switched off by means of the MOSFET transistors driven by MCU outputs PB2 and PB3. The output state is indicated by LEDs. When both devices are finally in the noiseless state, the Record Start signal on the MCU pin PB4 is generated and leads to the corresponding output connector and the LED indicator. The Record Start signal can be used for the quiet state indication in the case of manual operation or for the automated recording control. The audio level signal synchronous with the Record Start is passed to the synchronization output connector (Sync Out) as well. The Sync Out signal can be recorded on the dedicated audio track and subsequently used e.g. for the audio/video synchronization.

The presented version of the Fans-off device serves for the short-time switch-off of the cooling fans of the two instruments – the high-speed camera and the halogen light source. The number of the controlled devices can be easily extended, and the time sequence can be freely modified. More signal outputs for the audio/video recording and measurement device control and synchronization as well as additional trigger inputs can be added. The Fans-off device can be altered by the temperature sensors placed in the sensitive devices to monitor their actual temperature and avoid overheating.

4. The Fans-off Device experiment example

The necessity of the Fans-off device utilization is demonstrated here in a short overview of a violin research experiment (for more about experiment results and discovered causality see in full paper links [4, 6]).

The goal of the presented experiment example was to study different types of string movements (registered with a high-speed camera) in relation to listeners' aural perceptions while listening to the sound radiated from the violin (recorded with a microphone and audio recording equipment).

Generally, the high-speed camera recordings with short exposure times at high fps rates require a light source of high intensity. High-power lamps in general use are equipped with fans for active cooling. An additional cooling fan is usually embedded in the high-speed cameras as well. When running, the all fans produce a substantial

Figure 2: The recording of string movements and sounds

noise interfering with the sounds being recorded (for the noise spectrum example see Fig. 4).

In the presented experiment, the violin fixed in a frame holder was played with various bow speeds and bow pressures on a string to obtain various types of string vibrations.

The string movements were recorded using the high-speed camera Phantom SpeedSense 9060 (see Fig. 2). The camera video sensor chip and the electronics are cooled by the fan to reduce the sensor chip noise and to stabilize the camera parameters. The camera fan is covered with a perforated metal shield (the black rectangle at the left side of camera in Fig. 2).

The camera was located perpendicular to the violin top plate near the strings. The corresponding sounds were recorded using a dummy head (Neumann KU100) located in a similar way as the camera.

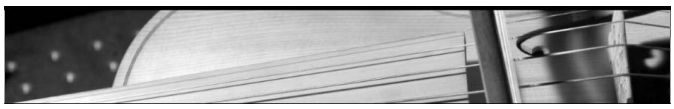

Figure 3: One recorded video frame

The measurement of the bowed string rapid movement required the video recording at a shutter speed of 60 kfps (for the sample of one video frame see Fig. 3). For the proper exposition at such a short shutter time the scene was illuminated by a powerful 1 kW halogen lamp equipped with a cooling fan. At the shutter speed of 60 kfps the maximum continuous recording time was limited by the camera internal memory size to approximately 1.5 s.

In the experiment, an absorbing panel was placed between the lamp stand and the camera mount (see Fig. 2). The panel kept the camera lens away from the direct lamp light and eliminated the first reflections of the sound waves, but the fan noises at the microphone position were not substantially affected.

To reach the goal of the presented experiment, the sounds of recorded violin tones are presented to listeners in psychoacoustical listening tests. The listeners are focused on the perception of different types of sound quality caused by certain string movements, but the perception of the recorded sound would be disturbed by the fans noise since the amplitude of prominent spectral components reached the SPL 50 dB and the SPL of the violin tones under examination was in the rage 60–80 dB (see Fig. 4). Due to the random character of the investigated violin sound components, neither the filtration nor the computational noise suppression techniques could be applied to suppress the interfering fan noises.

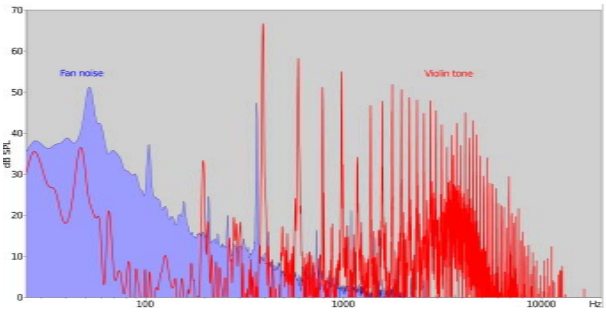

Figure 4: The violin tone and the fan noise spectra

To eliminate the fan noises from the sound recordings, the Fans-off device was applied. The device was programmed to switch on the sound recording after both the camera and the lamp fans stopped rotating (see the timing diagram with the corresponding fan noise levels time spans in Fig. 5).

The spin-off time of the lamp fan (Fan 1) was approximately 5 s. The spin-off time of the camera fan (Fan 2) was about 2.5 s. The recording time was 1.5 s.

The temperature build-up caused by shutting down the cooling fans was measured before the experiment.

The lamp surface temperature in the steady state was 53 °C. When the fan was switched off, the temperature started to rise with the rate of 3 °C per minute.

The camera internal temperature in the steady state reported by the control software was 55 °C. The temperature increase caused by the shutting down the fan for two minutes was 2 °C.

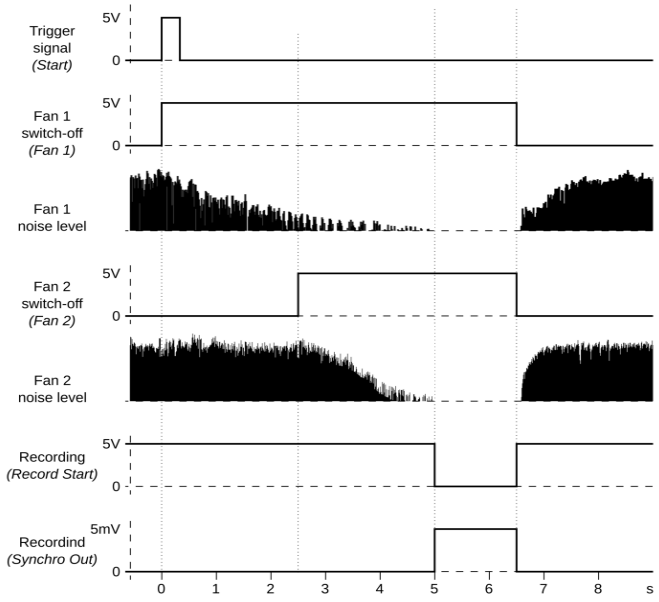

Figure 5: The signal sequence

The temperature measurements proved that the shutdown of both fans for up to one minute did not substantially change the equipment temperature. The about 15-minute-long camera memory readout and the storage of data to the external hard drive after each recording provides sufficient cooling time before the next recording session. Nevertheless, in the case of a 1.5 s recording time, a much shorter cooling time would be ample.

In the experiment example, the results of listening tests with the obtained noiseless recordings were correlated with suitable attributes describing the temporal courses of the string movements. Two examples of the acquired waveforms of string movement tracked near the bridge see in the Fig. 7 (the zoomed detail of the camera view used for movement tracking see in Fig. 6; for more about tracking and tracking software used see in [5]). For the detailed descriptions of the entire experiment and other type of waveforms see [4].

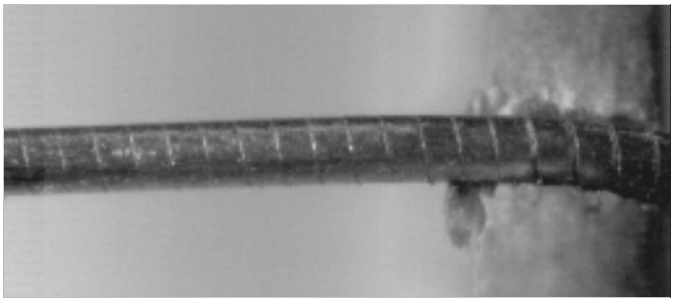

Figure 6: The detail of the string at the analyzed location (one video frame with the string near the bridge)

The presented experiment example results revealed a possible multi-dimensionality of perceived roughness

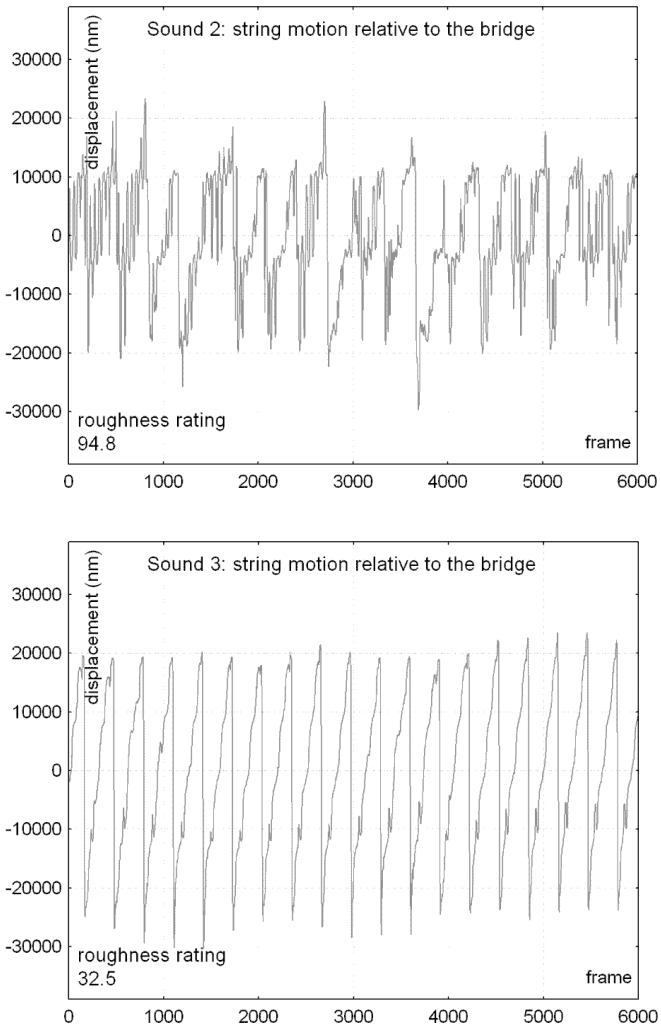

Figure 7: Two examples of temporal courses of the string movement near the violin bridge. Top: The tone with a large extent of the "cracked" percept. Bottom: The tone with a large extent of the "buzzing" percept

(more about correlations and results in [6]) which can be summarized in two basic findings: 1) the first dimension of perceived roughness (described by listeners with words globally represented by the term "cracked") is related to the irregular time changes of string movement amplitude (for the waveform irregularities see Fig. 7 top) and 2) the second dimension (described by the term "buzzing") is related to a very regular movement waveform (for the regular waveform, see Fig 7 bottom).

Without the use of the Fans-off device the high-quality audio recordings required for the unbiased listening tests results would not be achievable.

5. Conclusion

The results of the presented violin tone roughness experiment example would not have been obtained without the

use of the presented Fans-off device. The background noise level caused by the cooling fans was too high and it would have negatively affected the quality of the recorded audio samples used in the listening tests.

The Fans-off device has an essential importance in background noise elimination in the measurements and experiments utilizing a high-speed camera in combination with the requirement of simultaneous high-quality sound recordings.

The Fans-off device can also be helpful in the situations when the independent video and audio recordings need to be synchronized and the camera does not produce the required synchronization signal.

The presented microcontroller-based solution can be used for the timing of any electronically controlled unit, instrument or device during various measurements or experiments as well.

Acknowledgment

This research has been supported by the Ministry of Education, Youth and Sports of the Czech Republic in the Long Term Conceptual Development of Research Institutes grant of the Academy of Performing Arts in Prague: The "Sound quality" project.

References

[1] Deutschl, M., Guštar, M., Otčenášek, Z., Švec, J. G.: The influence of acoustic shields on voice measurements, In poster session 10th Pan European Voice Conference PEVOC, Prague 2013.

[2] How Effective Are Portable Vocal Booths? available at:
`http://www.soundonsound.com/sos/oct14/articles/vocal-booths.htm`

[3] Documentation: AVR ATtiny2313, Atmel, 2010, available at:
`http://www.atmel.com/images/doc2543.pdf`

[4] Otčenášek, Z., Otčenášek, J.: Perception of different Types of roughness of violin tones. In: Proceedings of the International Symposium on Musical Acoustics, July 7–12, 2014 – Le Mans, France. p. 557–62.
`http://zvuk.hamu.cz/vyzkum/publikacni.php`

[5] Software Tracker, available at:
`http://www.opensourcephysics.org/items/detail.cfm?ID=7365`

[6] Otčenášek, Z., Otčenášek, J.: Roughness of violin tones – perception of irregularities. In: Proceedings Third Vienna Talk, 16–19 Sept. 2015, Vienna.
`http://viennatalk2015.mdw.ac.at/?page_id=13002&pap=36`

Akustické listy: ročník 23, číslo 1–4 prosinec 2017 ISSN: 1212-4702
Vydavatel: Česká akustická společnost, z. s., Technická 2, 166 27 Praha 6 Vytisklo: Nakladatelství ČVUT, výroba
Počet stran: 24 Počet výtisků: 200
Redakční rada: M. Brothánek, O. Jiříček, J. Kozák, R. Čmejla, J. Volín
Jazyková úprava: R. Svobodová, M. Tharp

Uzávěrka příštího čísla Akustických listů je 29. ledna 2018.